Photocatalytic degradation of neonicotinoid insecticides using sulfate-doped Ag₃PO₄ with enhanced visible light activity

Youn-Jun Lee[a], Jin-Kyu Kang[b], Seong-Jik Park[c], Chang-Gu Lee[a,*], Joon-Kwan Moon[d,*], Pedro J.J. Alvarez[e]

[a] *Department of Environmental and Safety Engineering, Ajou University, Suwon 16499, Republic of Korea*
[b] *Environmental Functional Materials and Water Treatment Laboratory, Seoul National University, Republic of Korea*
[c] *Department of Bioresources and Rural System Engineering, Hankyong National University, Anseong, Republic of Korea*
[d] *Department of Plant Life and Environmental Sciences, Hankyong National University, Anseong, Republic of Korea*
[e] *Department of Civil and Environmental Engineering, Rice University, Houston, TX 77005, USA*

HIGHLIGHTS

- SO₄-Ag₃PO₄ catalyzed the removal of insecticides under visible light.
- Enhanced activity achieved by decreasing band gap and charge transfer resistance.
- Degradation followed the order of TCP > NTP > ICP > CTD > ATP > TMX > DTF.
- Mechanism mainly involves direct ICP oxidation by photoinduced hole.

ARTICLE INFO

ABSTRACT

Visible light-activated photocatalysts offer a promising approach to remove recalcitrant organic contaminants from water without adding chemicals, using free solar energy. In this study, sulfate-doped silver phosphate (SO₄-Ag₃PO₄) was prepared using a simple precipitation method, and its visible light photocatalytic activity against seven neonicotinoid insecticides currently available on the market was evaluated. The characteristics of the photocatalysts were analyzed using diffuse reflectance-UV/visible spectrophotometer measurements and electrochemical impedance spectroscopy analysis. Photocatalytic degradation of all tested insecticides under visible light irradiation was significantly enhanced by SO₄ doping, which decreased band gap energy and charge transfer resistance. The apparent first-order rate constant (k_{app}) with SO₄-Ag₃PO₄ varied depending on the insecticides (0.003–0.432/min), and was at least 5.4-fold faster than that with pristine Ag₃PO₄, in the order of thiacloprid (TCP) > nitenpyram (NTP) > imidacloprid (ICP) > clothianidin (CTD) > acetamiprid (ATP) > thiamethoxam (TMX) > dinotefuran (DTF). Even after four reuse cycles, SO₄-Ag₃PO₄ maintained over 75% of its initial photocatalytic efficiency. Reactive species trapping experiments indicated that photoinduced electron holes (h^+) were the most important oxidant for ICP degradation.

1. Introduction

Neonicotinoids are the most important commercial insecticides available in the global market, due to their high insecticidal activity, broad spectrum, adequate water solubility, and field stability. They are registered in more than 120 countries for use on more than 140 different crops [1,2]. Neonicotinoids were developed in the 1980s and the first commercial compound, imidacloprid (ICP), was patented by Bayer in 1985 and was successfully launched onto the market in 1991. They are highly active in controlling sucking pests including aphids, whiteflies, leafhoppers, planthoppers, thrips, some micro-lepidoptera, and many coleopteran pests [3,4]. Neonicotinoids bind strongly to nicotinic acetylcholine receptors (nAChRs) in the central nervous system as agonists and stimulate nerves at low concentrations, but at high concentrations (e.g., LC_{50} of 5 ng/bee) [5], they cause receptor blockage, paralysis, and death. Neonicotinoids are selectively more toxic to insect nAChRs, and are generally less toxic to mammals, birds, and fish [3,5]. Seven neonicotinoid insecticides that are currently available on the

market can be classified into three cyclic groups, five-membered ring systems (ICP and thiacloprid (TCP)), six-membered systems (thiamethoxam (TMX)), and noncyclic compounds (nitenpyram (NTP), acetamiprid (ATP), clothianidin (CTD), and dinotefuran (DTF)) [4].

With their widespread use, neonicotinoids are commonly detected in soil, surface water, and groundwater. The average total neonicotinoid concentrations in several rivers in Australia is 118 ng/L [1], while tap water in Iowa City, Iowa, USA, and Ontario, Canada, were reported to have concentrations of 57.3 and 280 ng/L, respectively [2]. The presence of neonicotinoids in water poses a treatment challenge due to their high solubility, recalcitrance to biodegradation, and persistence through wastewater treatment plants and constructed wetlands [1]. Thus, various technologies including bioaugmentation with specific bacteria, electrochemical degradation, hydrodynamic cavitation with hydrogen peroxide (H_2O_2), and ozonation (O_3) have been considered to degrade neonicotinoids [6–9]. However, these techniques have relatively low removal efficiency or suffer from the need for continued use of electricity and treatment chemicals. Photolysis has also been used to degrade various insecticides over the past decade [3]. For example, NTP, ICP, TMX, and CTD can be degraded by direct photolysis in both ultrapure and natural waters, while ATP was indirectly photolyzed mainly through reactions with hydroxyl radicals (•OH) [2]. Light-based processes including ultraviolet (UV) photolysis, UV/H_2O_2, UV/persulfate, UV/chlorine, and UV/titanium dioxide (TiO_2) approaches have been used for removing these contaminants from water [1,3,10]. Although photocatalytic degradation of ICP and TCP under visible light irradiation has also been reported [11], additional research is needed to understand pertinent degradation mechanisms (e.g., key oxidizing species) and inform photocatalytic material optimization.

Photocatalysis is one of the most widely researched treatment technologies because it uses light instead of chemicals as an ecofriendly approach to degrade organic pollutants [12]. There is growing interest in efficient visible-light-driven photocatalysts for the effective harvesting of solar energy to reduce the cost of water treatment processes [13]. Silver phosphate (Ag_3PO_4) has attracted significant attention as an efficient visible photocatalyst for water purification [14,15]. However, pristine Ag_3PO_4 has low efficiency in separating the photogenerated electron-hole pairs because of rapid recombination from narrow band gap, which reduces the photocatalytic activity. To address this obstacle, numerous attempts have been made to suppress the recombination rate of photogenerated electron-hole pairs by morphological modulation and heterojunction fabrication [11,16]. For example, sulfate-doped Ag_3PO_4 (SO_4-Ag_3PO_4), Ag_3PO_4@g-C_3N_4 hybrid composite, and Ag_2S-doped Fe_3O_4@Ag_3PO_4 nanostructures have been synthesized to enhance the visible light photocatalytic activity [11,13,17]. However, the relative efficiency of such photocatalysts to remove different types of neonicotinoid insecticides under visible light is unknown.

In this study, SO_4-Ag_3PO_4 was prepared as a visible-light-driven photocatalyst and its enhanced photocatalytic activity was evaluated through diffuse reflectance-UV/visible spectrophotometer measurements and electrochemical impedance spectroscopy analysis. Here, we compare the degradation of all seven neonicotinoid insecticides currently available on the market. The applicability and stability of the photocatalyst were evaluated and reductionist experiments were also conducted to discern the enhancement mechanisms and identify the main photogenerated oxidants in SO_4-Ag_3PO_4.

2. Material and methods

2.1. Chemicals

Silver nitrate ($AgNO_3$, ≥ 99.9%) was purchased from Kojima Chemicals Co. Ltd (Kashiwabara Sayama, Japan). Dibasic sodium phosphate (Na_2HPO_4, ≥ 99%) and sodium oxalate ($Na_2C_2O_4$, ≥ 99%) were purchased from Daejung Chemicals & Metals (Shiheung, Korea).

Sodium sulfate (Na_2SO_4, ≥ 98.5%), 1,4-benzoquinone ($C_6H_4O_2$, ≥ 98%), isopropyl alcohol ((CH_3)$_2$CHOH, ≥ 99.5%), methyl alcohol (CH_3OH, ≥ 99.5%), potassium nitrate (KNO_3, ≥ 99%), iron (III) nitrate nonahydrate (Fe(NO)$_3$·9H_2O, 98–102%), sulfuric acid (H_2SO_4, ≥ 95%), nitric acid (HNO_3, ≥ 70%), potassium hydroxide (KOH, ≥ 95%), and sodium azide (NaN_3 ≥ 99%) were purchased from Samchun Pure Chemical Co. Ltd (Pyeongtaek, Korea). Methyl orange (MO; $C_{14}H_{14}N_3NaO_3S$) was purchased from Junsei Chemical Co. Ltd (Japan). TiO_2 (denoted as P25) (≥99.5%), ATP ($C_{10}H_{11}ClN_4$, ≥ 99.9%), TCP ($C_{10}H_9ClN_4S$, ≥ 99.9%), ICP ($C_9H_{10}ClN_5O_2$, ≥ 98%), NTP ($C_{11}H_{15}ClN_4O_2$, ≥ 98.3%), and Reinecke's salt ($NH_4[Cr(NH_3)_2(SCN)_4]$, ≥ 93%) were purchased from Sigma-Aldrich Co. Ltd (St. Louis, MO, USA). CTD ($C_6H_5N_8SO_2Cl$, ≥ 99.5%) and TMX ($C_8H_{10}ClN_5O_3S$, ≥ 99.5%) were purchased from Chem Service Inc (West Chester, PA, USA). DTF ($C_7H_{14}N_4O_3$, ≥ 99%) was purchased from Wako Pure Chemical Industries, Ltd. (Osaka, Japan). Deionized water (18.2 MΩ/cm) from a Direct-Q, 3 UV system (Millipore, USA) was used for the preparation of all the solutions. All the chemicals were used as received without further treatment.

2.2. Catalyst preparation

The SO_4-Ag_3PO_4 catalyst was prepared using a modified precipitation method [17]. Five grams of $AgNO_3$ were dissolved in 1 L of ultrapure water. To this solution, 2.09 g of Na_2SO_4 was also added. After stirring for 30 min, this solution was added slowly into 500 mL of 0.02 M Na_2HPO_4 solution, while stirring vigorously. Subsequently, the mixture was stirred continuously for 2 h. Afterwards, the yellow precipitate was separated by centrifugation and washed thrice with ultrapure water, which was then dried at 70 °C for 12 h in a vacuum oven (FTVO-701, SCI FINETECH Co., Korea). Pristine Ag_3PO_4 was also prepared using the same synthetic procedure in the absence of Na_2SO_4.
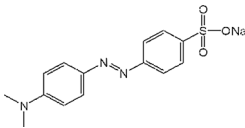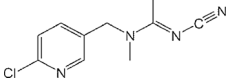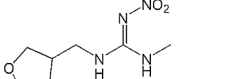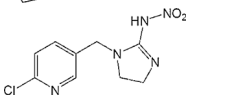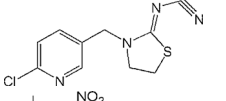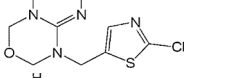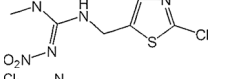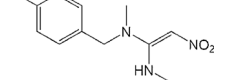
2.3. Characterizations

The surface morphologies and elemental compositions of the samples were observed through a transmission electron microscope (TEM) (Tecnai G2 F30 S-Twin, FEI, USA) and a field emission scanning electron microscope/energy dispersive spectrometer (FE-SEM/EDS) (JSM-6700F, JEOL). The crystal structure of the samples was determined using powder X-ray diffraction (XRD) (Rigaku D/max-2500 V/PC diffractometer, Rigaku, Japan). Nitrogen adsorption–desorption experiments were performed for evaluation of the specific surface areas, based on the Brunauer-Emmett-Teller (BET) theory, using the surface area analyzer (ASAP2420, Micromeritics, USA). Diffuse-reflectance spectra of the samples were measured using diffuse reflectance-UV/visible spectrophotometer (DRS) (S-4100, SCINCO, Korea) in the wavelength range of 300–800 nm. The electrochemical impedance spectroscopy (EIS) measurements were carried out by an electrochemical workstation (PGSTAT 302 N, Metrohm Autolab, Netherlands) in a three-electrode system. The Pt electrode acted as the counter electrode, the Ag/AgCl electrode was used as the reference electrode, and the working electrodes were prepared by coating the catalyst samples on a glassy carbon. The 0.5 M KNO_3 aqueous solution was used as the electrolyte. The X-ray photoelectron spectroscopy analysis (XPS) was performed to analyze the elemental chemical status of the samples using a SIGMA PROBE (Thermo Fisher Scientific, UK) with Al Kα radiation (hv = 1253.6 eV).

2.4. Experimental procedures

The photocatalytic activities of the prepared photocatalysts were evaluated by the degradation of the MO and the neonicotinoid insecticides (TCP, NTP, ICP, CTD, ATP, TMX, and DTF) under visible light irradiation. The chemical structure, molecular weight, and solubility (in water) of these chemicals are presented in Table 1. The visible light was

Table 1
Structure, molecular weight, and solubility (in water) of the chemicals used in this study.

Name	Molecular formula	Molecular structure	Molecular weight (g/mol)	Solubility in water (g/L)
Methyl orange (MO)	$C_{14}H_{14}N_3NaO_3S$		327.33	5
Acetamiprid (ATP)	$C_{10}H_{11}ClN_4$		222.67	4.2
Dinotefuran (DTF)	$C_7H_{14}N_4O_3$		202.214	39.8
Imidacloprid (ICP)	$C_9H_{10}ClN_5O_2$		255.662	0.51
Thiacloprid (TCP)	$C_{10}H_9ClN_4S$		252.72	0.185
Thiamethoxam (TMX)	$C_8H_{10}ClN_5O_3S$		291.71	4.1
Clothianidin (CTD)	$C_6N_5H_8SO_2Cl$		249.673	0.327
Nitenpyram (NTP)	$C_{11}H_{15}ClN_4O_2$		270.71	34.5

provided using six fluorescent lamps (4 W) placed in a black acrylic box. A quartz reactor equipped with a 420 nm cutoff filter was placed at a distance of 6 cm from the lamps. The light intensity determined by Reinecke's salt actinometry (λ = 446 nm) was 3.82×10^{-9} Einstein/cm^2/s, which corresponds to 1.03 mW/cm^2 (see SI Text S1 for details). Forty milligrams of the photocatalyst was added into 50 mL of the 15 µM MO and 5 mg/L of the neonicotinoid insecticide aqueous solutions. During the irradiation, 1 mL of aliquots were taken out and filtered with a 0.20 µm polytetrafluoroethylene (PTFE) filter (13JP020AN, Advantec, Japan) at specific time intervals. The adsorption experiment was carried out in the absence of the visible light source, while the photolysis experiment was conducted in the absence of the photocatalyst. The reusability of the photocatalyst was tested using the 15 µM MO solution. The aqueous suspension was centrifuged after 10 min of visible light irradiation and the supernatant was withdrawn. The precipitated photocatalyst was then suspended in the 15 µM MO solution for subsequent tests. The reusability tests were repeated for four times. Experiments were also conducted on two samples of natural waters collected from the secondary effluent from a municipal wastewater treatment plant located in Pyeongtaek, Korea (DOC = 4.71 ± 0.09 mg/L, Table S1) and from a lake located in Suwon, Korea (DOC = 2.67 ± 0.02 mg/L, Table S1), with spiking ICP (5 mg/L). The reactive oxygen species (ROS) trapping experiments were conducted separately by adding 0.5 mM ROS scavengers (*p*-benzoquinone, sodium azide, sodium oxalate, isopropyl alcohol, and methanol) into the 5 mg/L of ICP solutions. The generation of ROS species was further investigated by an electron paramagnetic resonance (EPR) spectrometer (JES-FA200, JEOL, Japan). The test was conducted in the black acrylic box where the photocatalytic experiments were performed. 5,5-dimethyl-1-pyrroline-N-oxide (DMPO) and 2,2,6,6-tetramethyl-4-piperidone (TEMP) were used as spin traps. Spin traps were added into the 2 mL, 0.8 g/L of photocatalyst suspension. Then, the visible light was

irradiated to the sample for 5 min.

2.5. Analytical methods

The concentration of MO was analyzed using a UV/visible spectrophotometer (NEO-S2117, NEOGEN, Korea) at a wavelength of 480 nm. An Agilent 1100 Series HPLC system (Agilent Technologies Inc., USA) with a solvent degassing unit, a binary pump, an autosampler, a column compartment, and a diode array detector (DAD) was used for the analysis of neonicotinoid insecticides. Separation of the compounds was achieved on a Phenomenex Luna C18 column (250 mm × 4.6 mm, 5 µm particle size) with a column temperature of 25 °C. The two mobile phases of acetonitrile (ACN) (A) and water (B) were delivered at the flow rate of 1.0 mL/min. The gradient mode was initially set at an A/B ratio of 15:85 from 0 to 2 min, later was linearly increased to a ratio of 50:50 at 10–12 min and finally to 15:85 at 15–20 min. The DAD detection wavelengths were set at 246 nm for ATP, TMX, and TCP, and at 270 nm for CTD, DTF, ICP, and NTP. The injection volume was 10 µL. Concentrations of neonicotinoids were calculated using the regression equation of their concentration and peak area based on the retention times. The dissolved organic carbon (DOC) was determined by a DOC analyzer (TOC-VCSN, Shimadzu, Japan). Shimadzu LCMSMS-8040 system (Shimadzu, Japan) coupled with Nexera XR LC-20AD, SIL-20A, SPD-20A, and CTO-20A was used to analysis and identification of degradation products. The mobile phase A was water containing 0.1% formic acid, and mobile phase B was acetonitrile with 0.1% formic acid. The analytical column was Capcell Core C18 (2.1 × 150 mm, 2.7 µm particle size, OSAKA SODA, Japan). The gradient mobile phase was consisted of 0–1 min, 10%B; 15–20 min, 60%B; 21–25 min, 10%B. Flow rate was 0.2 mL/min and column oven temperature was 40 °C. Injection volume was 2 µL and total runtime was 20 min. Gas flow rate of nebulizing and drying was 3 and 15 L/min,
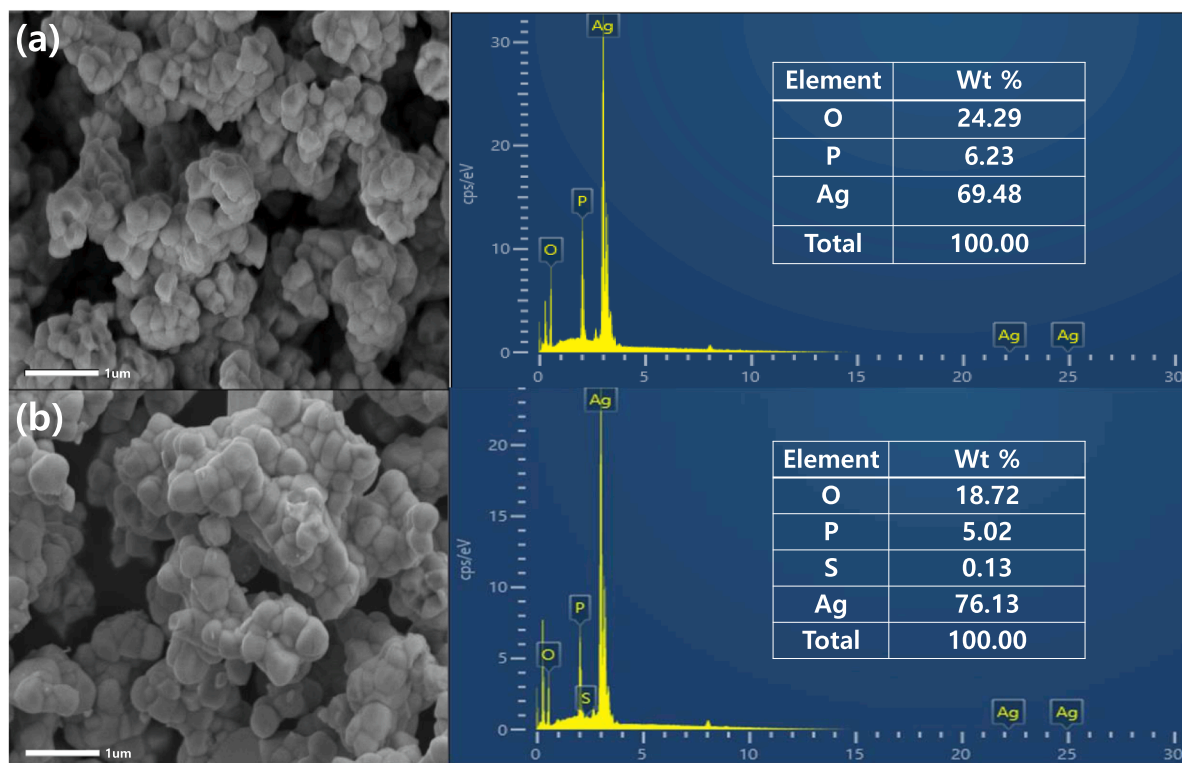
Fig. 1. Fe-SEM images of (a) Ag_3PO_4 and (b) SO_4-Ag_3PO_4 with EDS analysis.

respectively. For the identification of degradation product, electrospray ionization (ESI), MS scan with positive or negative mode, and MS product mode with 230 kPa collision-induced dissociation (CID) gas and −25 CE voltage was used. All experiments were performed in duplicate and one tailed *t*-test was used to determine statistically significant differences between treatments at the 95% confidence level ($p < 0.05$).

3. Results and discussion

3.1. Characterization of Ag_3PO_4 and SO_4-Ag_3PO_4

To investigate the surface morphology and chemical composition of the prepared samples, the Fe-SEM microscopies of Ag_3PO_4 and SO_4-Ag_3PO_4 were measured using EDS analyses. Fig. 1(a) shows the interconnected, irregular, particle-like shape of Ag_3PO_4, which consisted of silver (69.48 wt%), oxygen (24.29 wt%), and phosphorus (6.23 wt%). There was no significant change in the morphology after the introduction of sulfate (Fig. 1(b)), which was attributed to the low sulfur content (0.13 wt%) [17]. Even though the sulfur content is low, it made a significant difference in the photocatalytic degradation, as discussed in the next section. The index for the body-centered cubic structure of Ag_3PO_4 (JCPDS No. 06–0505) was measured by XRD analysis of both samples (Fig. S1). Sulfate doping did not affect the crystal structure and no impurities were observed. The TEM analysis was also performed to further ascertain the Ag_3PO_4 and SO_4-Ag_3PO_4. The nanosized particles had sizes ranging from 20 to 60 nm (Fig. 2) and were smaller than the typical size of Ag_3PO_4 reported in previous studies (200–500 nm) [13,17,18], but were similar to the Ag_3PO_4 nanocrystal on the graphene sheets (20–50 nm) [19]. The lattice fringes were also clearly identified in both samples through TEM analysis. The lattice fringe spacing of samples were 0.245 nm and 0.246 nm, corresponding to the (2 1 1) crystal plan of Ag_3PO_4 [20], which is consistent with XRD results. The specific surface area calculated through BET analysis (Fig. S2) decreased slightly from 1.08 m^2/g to 0.85 m^2/g with the introduction of

sulfate. Deconvoluted spectra of SO_4-Ag_3PO_4 and reused SO_4-Ag_3PO_4 are presented in Fig. 8. From the S 2p high resolution, the peak at 168.4 eV contributed from S^{6+} is the evidence of SO_4 doping into the Ag_3PO_4 lattice [17].

3.2. SO_4-Ag_3PO_4 significantly outperformed Ag_3PO_4 under visible light irradiation

Photocatalytic activity of the prepared samples under visible light for methyl orange (MO) degradation is benchmarked against commercial TiO_2 (Fig. 3(a)), which is the most commonly used semiconductor photocatalyst [21]. MO degradation by Ag_3PO_4 and SO_4-Ag_3PO_4 were faster than P25 because Ag_3PO_4 is generally efficient in dye removal under visible light irradiation while P25 (which requires UV for activation) is not [15]. SO_4-Ag_3PO_4 exhibited the highest photocatalytic activity, and completely removed the MO dye in 10 min under visible light irradiation. In contrast, the Ag_3PO_4 removed 57.0 ± 3.1% of the MO in 20 min, while only 14.7 ± 2.7% of the dye was removed by P25 in 20 min. The effect of SO_4 content on photocatalytic efficiency of SO_4-Ag_3PO_4 was also considered (Fig. S3), and the results were in agreement with literature [17]. Photolysis (visible light only) of the MO dye did not occur and adsorption (in the dark) by the three photocatalysts was negligible (Fig. 3(b)). This indicates that MO degradation was solely due to photocatalytic activity.

To elucidate the reasons for the improved photocatalytic activity by introducing sulfate, the DRS and EIS analyzes were performed for Ag_3PO_4 and SO_4-Ag_3PO_4. The DRS of the undoped (control) and doped samples are shown in Fig. 4(a). The photocatalysts showed strong photo-adsorption at wavelengths below 530 nm, corroborating their photocatalytic activity under visible light irradiation [13,22]. Moreover, the photo-absorption intensity of the photocatalyst was enhanced in the region of 530–800 nm by sulfate doping, which made the color of the photocatalyst darker. Accordingly, SO_4-Ag_3PO_4 could adsorb more photons than Ag_3PO_4 [23,24]. The band gap energies (E_g) of the samples were estimated by modified Kubelka–Munk function using the
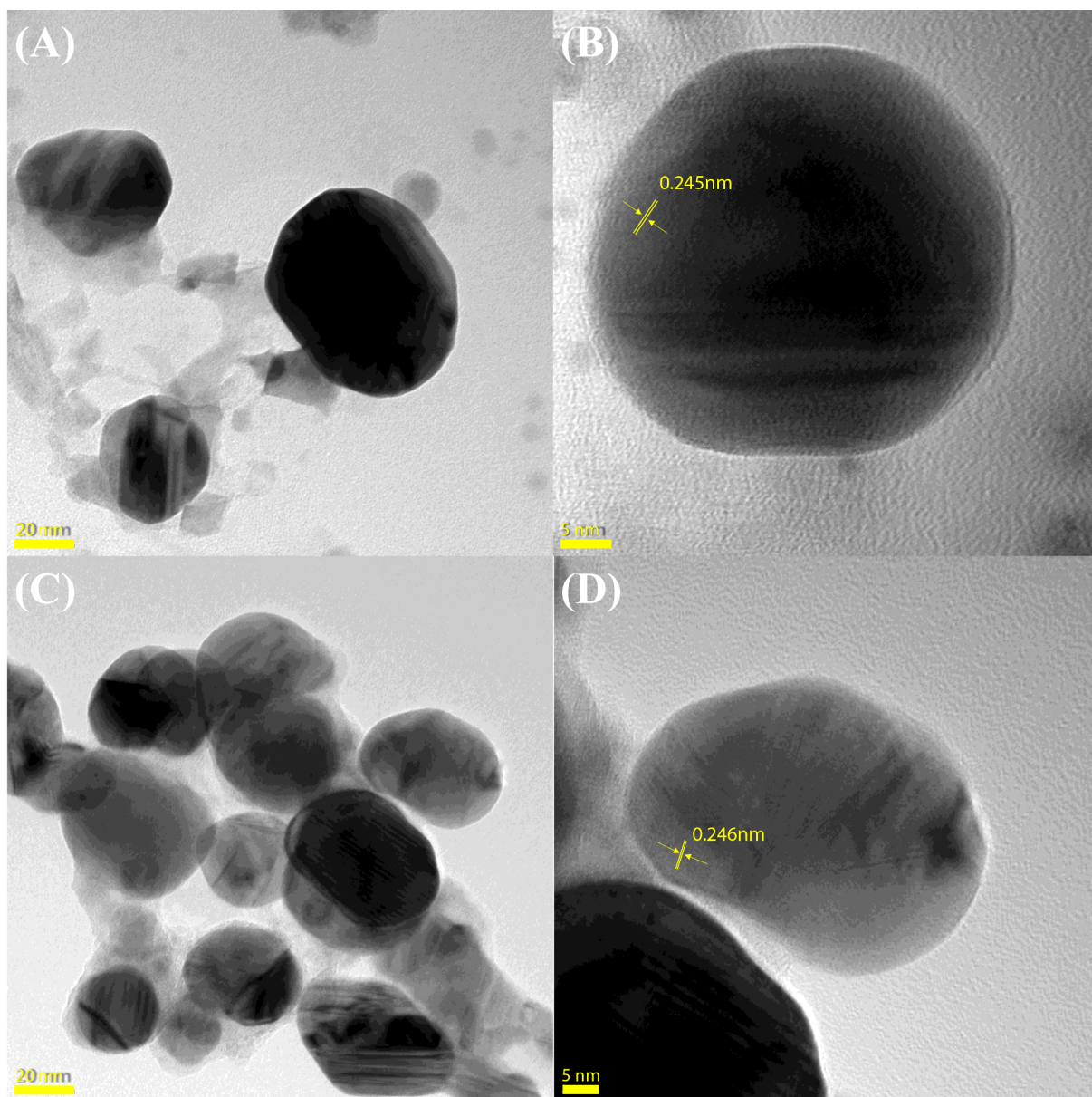
Fig. 2. TEM images of (a, b) Ag_3PO_4 and (c, d) SO_4-Ag_3PO_4.

following formula [17,25]:

$$\alpha h\nu = A(h\nu - E_g)^{n/2} \tag{1}$$

where h and ν are the Planck constant and the light frequency, respectively. α and A are the absorption coefficient and absorption constant, respectively. Parameter n, depends on the transition properties of the semiconductor and is kept as 4 since Ag_3PO_4 is considered as an indirect band gap semiconductor. Thus, E_g could be estimated from the tangent line x-intercept of the plot of $(\alpha h\nu)^{1/2}$ versus photon energy ($h\nu$). The band gap energy (E_g) of Ag_3PO_4 was 2.25 eV (Fig. 4(b)), which was consistent with the literature [25,26]. The E_g of SO_4-Ag_3PO_4 was 2.14 eV (Fig. 4(c)), which was lower than that of pure Ag_3PO_4. The results demonstrate that sulfate doping can reduce the band gap of Ag_3PO_4, hence reducing the energy required for photoactivation [27]. In addition, EIS was used to probe the separation efficiency of the electron-hole pairs under visible light irradiation. Generally, the smaller radius of the arc in an EIS Nyquist plot corresponds to a smaller charge transfer resistance [13,24]. The arc radius of SO_4-Ag_3PO_4 was smaller than that of Ag_3PO_4 (Fig. 5). This indicates that the sulfate

doping decreased the charge transfer resistance of Ag_3PO_4 and improved charge transfer efficiency [11,17]. Together with the observed reduced bandgap energy, this corroborates the increased photocatalytic activity of Ag_3PO_4 conferred by sulfate doping. Meanwhile, since S atom has more valence electrons than P atom, doping SO_4 into the Ag_3PO_4 lattice results in an n-type semiconductor capable of providing additional electrons. This n-type doping can improve photocatalytic activity by increasing carrier concentration and intrinsic conductivity [28].

3.3. Application to neonicotinoid insecticides degradation

The prepared photocatalysts were applied to the photocatalytic degradation under visible light irradiation for different neonicotinoid insecticides such as TCP, NTP, ICP, CTD, ATP, TMX, and DTF. SO_4-Ag_3PO_4 performed better in removing the insecticides compared with Ag_3PO_4, for all the pesticides tested (Fig. 6). The kinetics of the photocatalytic degradation of the insecticides could be described by pseudo first-order kinetics [11,29]:
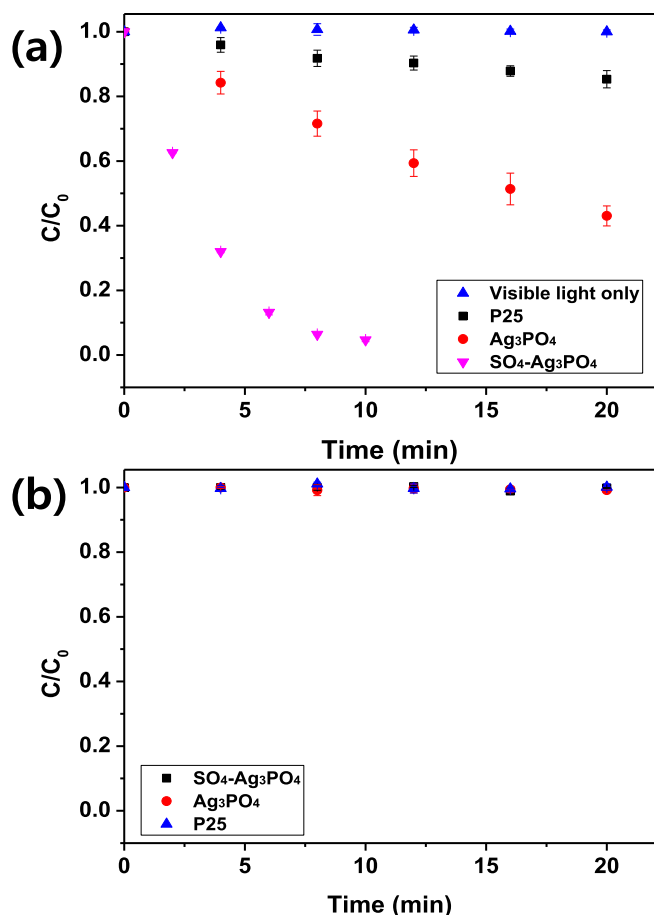
Fig. 3. (a) Photocatalytic degradation of methyl orange ($[MO]_0$ = 5.6 mg/L) by P25, Ag_3PO_4, and SO_4-Ag_3PO_4 under visible light (1.03 mW/cm^2) and (b) adsorption in the dark. Error bars represent ± one standard deviation from the mean of triplicate measurements. Error bars smaller than symbols are not depicted. (For interpretation of the references to color in this figure legend, the reader is referred to the web version of this article.)

$$ln\left(\frac{C}{C_0}\right) = -k_{app}t \tag{2}$$

where C and C_0 are the concentrations at time t and 0, respectively, and k_{app} is the apparent first-order rate constant (Table 2). The k_{app} of SO_4-Ag_3PO_4 varied from 0.003 ± 0.000/min to 0.432 ± 0.020/min, depending on the insecticide, although they were tested at the same initial concentration (C_0 = 5 mg/L). The degradation rate of the insecticides by SO_4-Ag_3PO_4 were in the order of TCP > NTP > ICP > CTD > ATP > TMX > DTF and these values were at least 5.4 times faster than the degradation rate by Ag_3PO_4 for each insecticide. The adsorption of insecticides by the photocatalysts in the dark was negligible (Fig. S4(a) and (b)) and the photolysis (visible light only) was not sufficient in our experimental conditions, except for NTP (k_{app} = 0.063 ± 0.002/h) (Fig. S4(c)).

It should be noted that the apparent first-order rate constant (k_{app}) calculated in this study is difficult to directly compare with other photocatalytic studies due to different experimental setups and conditions [3]. However, this study compared all seven neonicotinoid insecticides currently available on the market under the same experimental conditions, so it is worth mentioning that the difference in the calculated rate constant is not due to the uncertainties of the experimental setups, but to the chemical properties of the selected compounds. First, the diversity of structures can affect the degradation of neonicotinoid insecticides. In general, two five-membered cyclic compounds (TCP and ICP) are effectively degraded by advanced oxidation
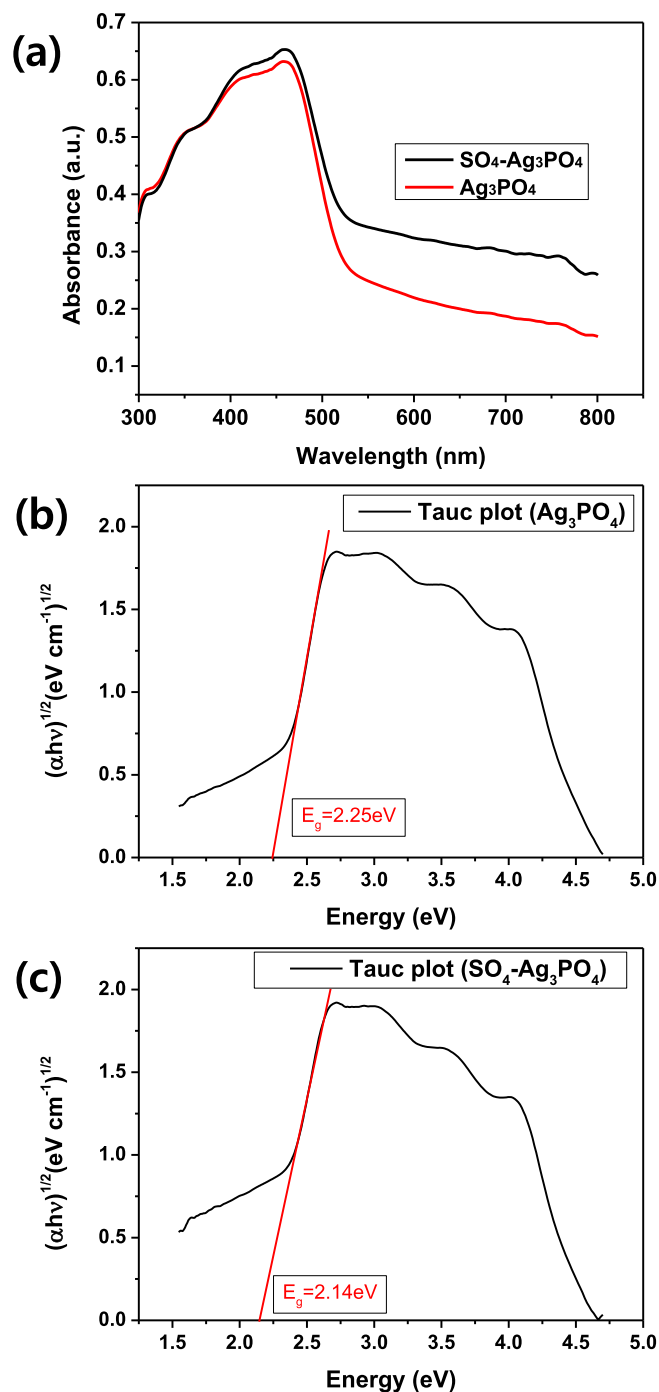

Fig. 4. (a) UV–vis diffuse reflectance spectra of Ag_3PO_4 and SO_4-Ag_3PO_4 and modified Kubelka-Munk function versus light energy for band gap energies of (b) Ag_3PO_4 and (c) SO_4-Ag_3PO_4.

processes (AOPs) [30–34], where non-cyclic compounds with long aliphatic chains (CTD and ATP) are well-known to be less prone to be oxidized [29]. On the other hand, photostability can also be used to account for different rate constants. Thus, NTP, a nitromethylene functional groups ([=CH–NO$_2$]), is more susceptible to photolysis than compounds with an N-nitroguanidine functional groups ([=N–NO$_2$]), ICP, CTD, TMX and DTF, whereas ATP, an N-cyanoamidine functional groups ([=N–CN]), is stable to irradiation [4,10].

In our case, the degradation of TCP (0.432 ± 0.020/min) and NTP (0.266 ± 0.008/min) by SO_4-Ag_3PO_4 were rapid among the tested neonicotinoid insecticides, with 88.64 ± 1.84% and 73.66 ± 0.94%
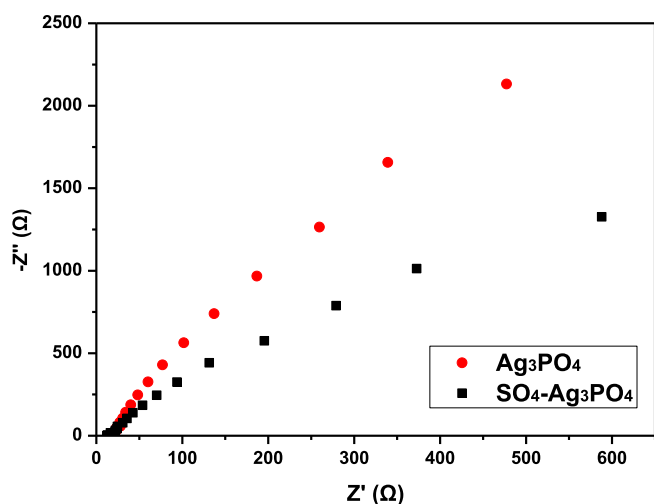
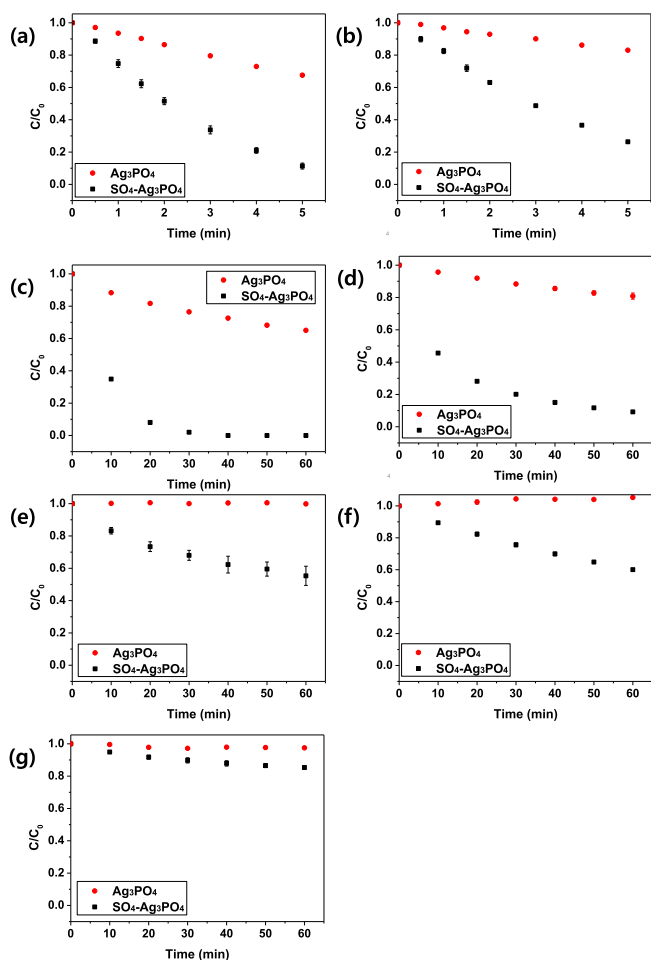**Fig. 5.** Electrochemical impedance spectroscopy (EIS) Nyquist plot of Ag₃PO₄ and SO₄-Ag₃PO₄.

Fig. 6. Photocatalytic degradation of neonicotinoid insecticides (C$_0$ = 5 mg/L) under visible light (1.03 mW/cm^2) by Ag₃PO₄ or SO₄-Ag₃PO₄: (a) thiacloprid (TCP), (b) nitenpyram (NTP), (c) imidacloprid (ICP), (d) clothianidin (CTD), (e) acetamiprid (ATP), (f) thiamethoxam (TMX), and (g) dinotefuran (DTF). Error bars represent ± one standard deviation from the mean of triplicate measurements. Error bars smaller than symbols are not depicted.

removal within 5 min, respectively. NTP reacts very quickly under sunlight and undergoes direct photolysis [2], while TCP is relatively stable to photolysis [2,10]. Meanwhile, ICP, CTD, ATP, TMX, and DTF

Table 2
Degradation rate constants (k_{app}) for the tested pesticides, using Ag₃PO₄ or sulfate-doped Ag₃PO₄.

	SO₄-Ag₃PO₄		Ag₃PO₄	
	k_{app} (/min)	R^2	k_{app} (/min)	R^2
MO	0.329 ± 0.019	0.983	0.042 ± 0.001	0.999
TCP	0.432 ± 0.020	0.985	0.080 ± 0.001	0.998
NTP	0.266 ± 0.008	0.994	0.038 ± 0.001	0.997
ICP	0.132 ± 0.006	0.993	0.007 ± 0.001	0.970
CTD	0.038 ± 0.004	0.937	0.004 ± 0.000	0.990
ATP	0.009 ± 0.001	0.944	n.a.[†]	n.a.
TMX	0.008 ± 0.000	0.995	n.a.	n.a.
DTF	0.003 ± 0.000	0.937	n.a.	n.a.

[†] n.a.: not applicable.

were removed by SO₄-Ag₃PO₄ within 60 min, with removal efficiencies of 99.66 ± 0.34%, 90.78 ± 0.10%, 44.67 ± 5.94%, 39.94 ± 0.81%, and 14.64 ± 1.07%, respectively, under visible light irradiation. ICP completely disappeared within 40 min (Fig. 6(c), detection limit = 2.58 μg/L). However, mineralization is rarely achieved with AOPs [35–37], raising the possibility that more bioavailable or more toxic byproducts could be formed. Thus, even though results are encouraging from a regulatory compliance perspective, further tests are recommended to assess detoxification as a function of treatment time and intensity. The photocatalytic degradation of DTF by SO₄-Ag₃PO₄ under visible light irradiation was the slowest among the tested neonicotinoid insecticides. Information on the degradation of DTF in aqueous solution is very limited and only a few studies on photolysis have been reported [38,39].

3.4. Stability and applicability of SO₄-Ag₃PO₄

The stability of the photocatalyst is very important for their practical applications [17,19]. Therefore, the photocatalytic stability of SO₄-Ag₃PO₄ under visible light irradiation was investigated by collecting the used sample after photocatalysis and performing the reuse experiments under the same conditions for four cycles. SO₄-Ag₃PO₄ was able to completely remove MO within 10 min of visible light irradiation in the first cycle (Fig. 7). The apparent degradation rate was 0.329 ± 0.019/min, which was 7.8 times higher than that of Ag₃PO₄ (0.042 ± 0.001/min). The photocatalytic performance gradually decreased and 75.2% of the MO was removed within 10 min after the four reuses. The decrease in photocatalytic activity was attributed generally
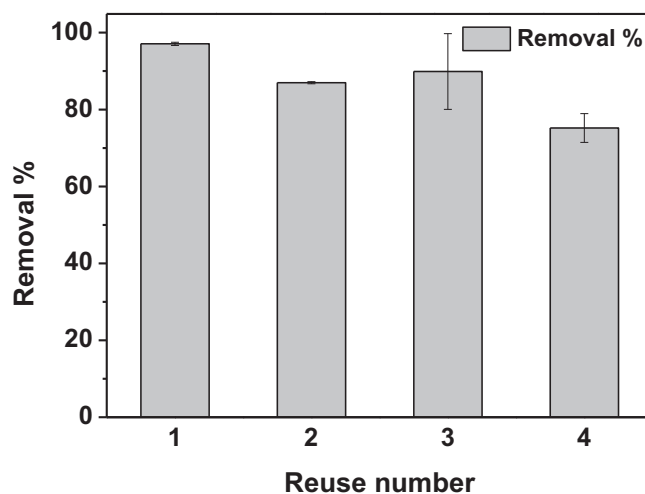

Fig. 7. Reuse of SO₄-Ag₃PO₄ over four cycles to remove methyl orange for 10 min under visible light (1.03 mW/cm^2) ([MO]$_0$ = 5.585 mg/L). Error bars represent ± one standard deviation from the mean of triplicate measurements.

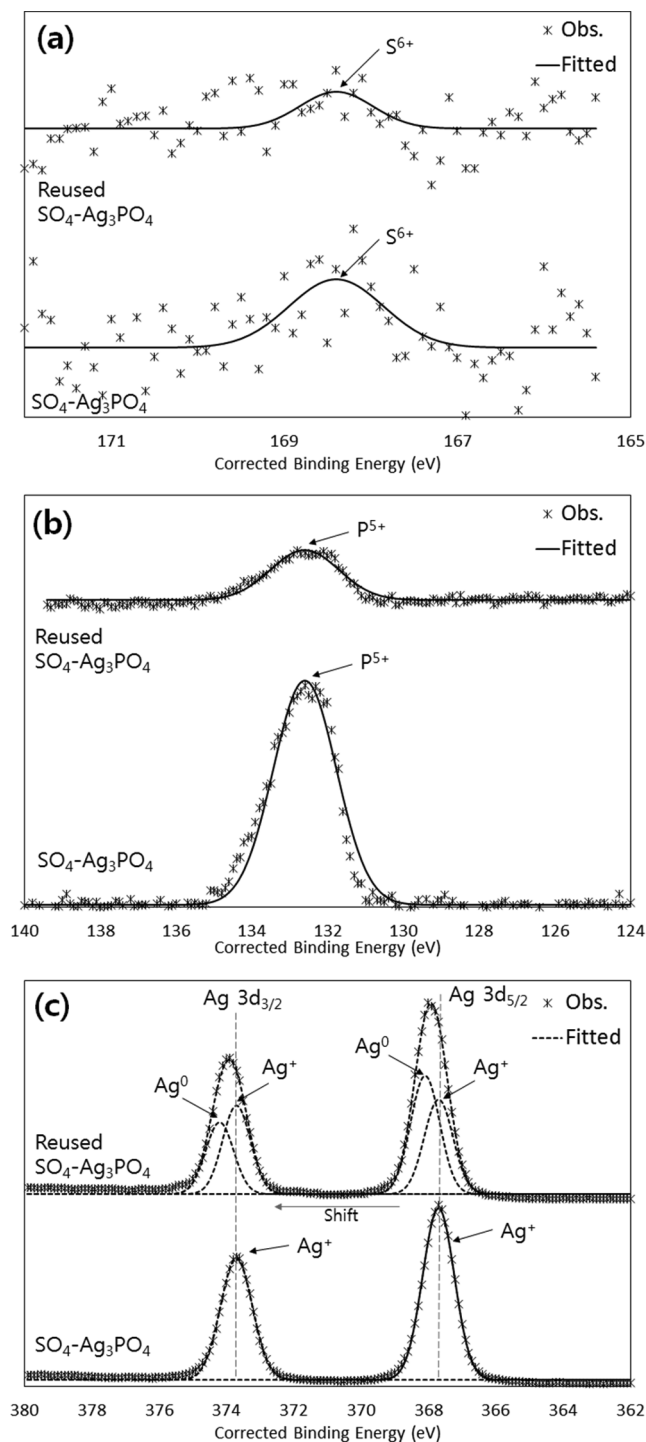**Fig. 8.** High-resolution XPS spectra of SO_4-Ag_3PO_4 and reused SO_4-Ag_3PO_4: (a) S 2p, (b) P 2p, (c) Ag 3d.

Fig. 9. (a) SO_4-Ag_3PO_4 photocatalytic degradation of imidacloprid ($[ICP]_0 = 5$ mg/L) in the secondary effluent from the municipal wastewater treatment plant and the lake water under visible light (1.03 mW/cm^2) and (b) effect of different scavengers on photocatalytic degradation of imidacloprid ($[ICP]_0 = 5$ mg/L) by SO_4-Ag_3PO_4. Error bars represent $\pm$ one standard deviation from the mean of triplicate measurements. Error bars smaller than symbols are not depicted.

to the reduction of partial silver ion (Ag^+) to silver atoms (Ag^0) during the photocatalytic reaction. The electrons generated by absorbing photons combine with an interstitial Ag^+ to produce Ag^0, causing photocorrosion of photocatalyst in the absence of a sacrificial reagent [40]. From the Ag 3d high resolution (Fig. 8(c)), the two peaks were described as the binding energies of Ag 3d5/2 and Ag 3d/2 at about 368 and 374 eV, respectively. Only the peaks of SO_4-Ag_3PO_4 were deconvoluted into Ag^+, while the peaks of reused SO_4-Ag_3PO_4 were shifted into higher binding energy and deconvoluted into Ag^+ and Ag^0 according to the XPS results from previous studies of Ag_3PO_4 [41,42]. In addition, the peak at 132.6 eV in P 2p is also considered as a
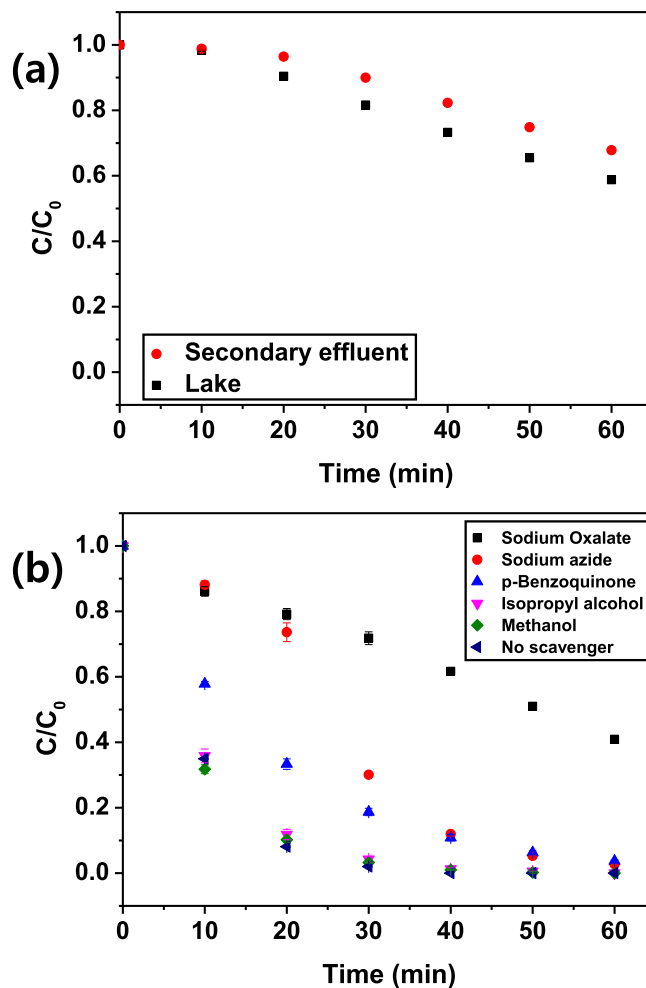
contribution of P^{5+} to Ag_3PO_4, though the P^{5+} and S^{6+} peaks' intensities were reduced after reuse (Fig. 8(b)). Nevertheless, the k_{app} of SO_4-Ag_3PO_4 after the four reuses (0.125/min) was still higher than that with pristine Ag_3PO_4, and no apparent crystalline structure changes were observed in the XRD pattern after the reuse experiment (Fig. S1), indicating the stability of SO_4-Ag_3PO_4 photocatalyst.

To investigate the potential interference of background organics present in the water, the photocatalytic degradation of ICP in the secondary effluent from the municipal wastewater treatment plant and the lake water was evaluated (Fig. 9(a)). The photocatalytic activity was significantly ($p < 0.05$) reduced in both the water samples and the further decrease in the secondary effluent was due to the higher DOC (4.71 ± 0.09 mg/L) and UV_{254} (0.100 ± 0.000) values compared with the lake water (DOC = 2.67 ± 0.02 mg/L, $UV_{254} = 0.050 \pm 0.001$, Table S1). The reduction of photocatalytic activity by the background organics could be explained in two ways. Background organics not only absorb light and hinder light delivery to the photocatalyst, but also act as ROS scavengers and interfere with the degradation of the target contaminants [10]. This hindrance could be overcome by additional pretreatment using advanced treatment techniques [1] and/or by immobilizing the photocatalyst on a suitable substrate that concentrates the target contaminants near photocatalytic

sites (named "trap-and-zap" strategy) [21,43].

3.5. Degradation mechanism mainly involves direct ICP oxidation by photoinduced holes

Reactive species trapping experiments were conducted to elucidate the main oxidants responsible for ICP degradation by SO_4-Ag_3PO_4 under visible light irradiation, including hydroxyl radical (•OH), superoxide radicals (•O_2^-), singlet oxygen ($^1O_2$) and photoinduced electron holes (h^+) [24,44]. In these experiments, methanol or isopropyl alcohol, p-benzoquinone, sodium azide, and sodium oxalate were used as the scavengers of •OH, •O_2^-, $^1O_2$, and h^+, respectively. The addition of methanol, isopropyl alcohol, or p-benzoquinone had no apparent effect on photocatalytic degradation of ICP (Fig. 9(b)). In contrast, addition of sodium azide and sodium oxalate significantly ($p < 0.05$) suppressed photocatalytic degradation of ICP by SO_4-Ag_3PO_4, of which the sodium oxalate was more pronounced. This indicates that the photoinduced holes (h^+) are the most important reactive species in this system, which is consistent with the results of the reactive species trapping experiments of pure Ag_3PO_4 reported in previous studies [17,24,45]. To further verify reactive species, EPR technique was employed to prove the generation of •OH, •O_2^-, and $^1O_2$. DMPO was used to trap •OH and •O_2^-, while TEMP was applied for $^1O_2$ [46,47]. As shown in Fig. 10(a), no signal was observed in the dark, and •OH-DMPO and •O_2^--DMPO characteristic peaks were not observed under visible light irradiation. These results were in good agreement with the results of the trapping experiments. Meanwhile, intensive triplet characteristic peaks for $^1O_2$-TEMP was observed under visible light irradiation, indicating that $^1O_2$ could be generated in our system. Despite the low rate constants observed for the reaction between singlet oxygen and neonicotinoid insecticides, a reaction mechanism was found that involved charge transfer from the insecticide to $^1O_2$ [48]. Thus, the following equations (Eqs. (3)-(7)) can be used to describe the possible photocatalytic reactions [47,49,50]. Nevertheless, since the effect of p-benzoquinone that can suppress the generation of $^1O_2$ was insignificant, $^1O_2$ may have a minor effect on the photocatalytic degradation of ICP. Therefore, the ICP oxidation mechanism by SO_4-Ag_3PO_4 predominantly involved a direct attack by h^+, and the possible photocatalytic degradation mechanism can be illustrated as following (Fig. 10(b)).
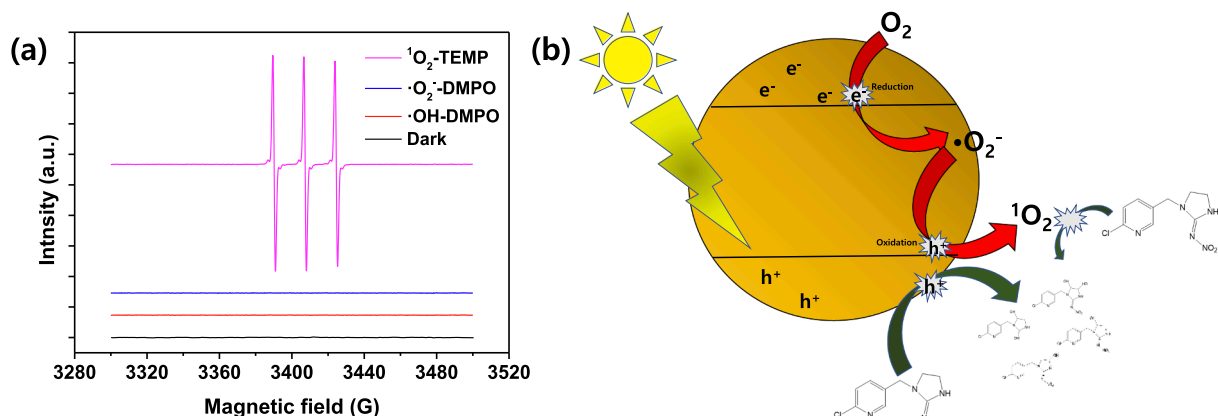
$$Catalyst + visible\ light \rightarrow h^+ + e^- \tag{3}$$

$$e^- + O_2 \rightarrow \cdot O_2^- \tag{4}$$

$$\cdot O_2^- + h^+ \rightarrow {}^1O_2 \tag{5}$$

$$Organic\ matter + h^+ \rightarrow products \tag{6}$$

$$Organic\ matter + {}^1O_2 \rightarrow products \tag{7}$$

Detailed products analyses for photocatalytic degradation of ICP by SO_4-Ag_3PO_4 were performed. Three major degradation products were present in the chromatogram with PDA detector and LC-MSMS full scan chromatogram at positive or negative mode (Fig. S5). The biggest peak was ICP with molecular ion plus proton $[M + H]^+$ peak at 256 m/z, $[M + 2 + H]^+$ peak at 257 m/z because of chlorine in positive mode. At the negative mode, molecular ion minus proton $[M - H]^-$ peak at 254 m/z and $[M + 2\text{-}H]^-$ peak at 256 m/z were detected (Fig. S6). The MS product scan mode was used to identify the structure of parent ion and the m/z values with major fragment ions are shown in Table S2. The product of $m/z = 256$ were $m/z = 209, 175, 146, 133, 128, 126$, and 84. The daughter of $m/z = 209$ was loss of Cl and $m/z = 175$ was ICP loss of Cl and NO_2. Metabolite I was tentatively 3-((6-chloropyridin-3-yl)methyl)imidazolidine-2,4-diol, with molecular ion plus proton $[M + H]^+$ peak at 230 m/z, $[M + 2 + H]^+$ peak at 232 m/z in positive mode. At the negative mode, molecular ion minus proton $[M - H]^-$ peak at 228 m/z and $[M + 2\text{-}H]^-$ peak at 230 m/z were detected (Fig. S7). The product of $m/z = 230$ were $m/z = 186, 169, 147, 132$, and 126. Metabolite II was dihydroxy imidacloprid with molecular ion plus proton $[M + H]^+$ peak at 288 m/z, $[M + 2 + H]^+$ peak at 290 m/z in positive mode. At the negative mode, molecular ion minus proton $[M - H]^-$ peak at 286 m/z, $[M + 2\text{-}H]^-$ peak at 288 m/z, and $m/z = 228$ from loss of nitro-amine were detected (Fig S8). The product of $m/z = 288$ were $m/z = 241, 223, 207, 189, 183, 169, 161, 149, 132$, and 126. The daughter of $m/z = 126$ was (6-chloropyridinyl)benzyl ion that means hydroxylation was reacted at the imidazolidine ring [51,52]. Metabolite III was mono-hydroxy imidacloprid with molecular ion plus proton $[M + H]^+$ peak at 272 m/z, $[M + 2 + H]^+$ peak at 274 m/z in positive mode. At the negative mode, molecular ion minus proton $[M - H]^-$ peak at 270 m/z and $[M + 2\text{-}H]^-$ peak at 272 m/z were detected (Fig. S9). The product of $m/z = 272$ were $m/z = 225, 207, 191, 183, 174, 172, 161, 146, 134$, and 126. The daughter of $m/z = 126$ was (6-chloropyridinyl)benzyl ion that means hydroxylation was reacted at the imidazolidine ring as metabolite II. The daughter of $m/z = 225$ was from loss of nitro group, and $m/z = 191$ was loss of Cl and NO_2. Based on these identified products from mass spectrometer, the degradation pathways of ICP by SO_4-Ag_3PO_4 under visible light irradiation are shown in Fig. 11.

4. Conclusions

SO_4-Ag_3PO_4 was prepared using a facile precipitation method to enhance the photocatalytic activity of the catalyst and degrade neonicotinoid insecticides under visible light irradiation. Results demonstrate that the sulfate doping reduces the band gap; hence, it could reduce the energy

Fig. 10. (a) EPR spectra of •OH-DMPO, •O_2^--DMPO and $^1O_2$-TEMP in the presence of SO_4-Ag_3PO_4 under visible light irradiation and in the dark. (b) Schematic mechanism of reactive species for photocatalytic degradation of ICP by SO_4-Ag_3PO_4 under visible light irradiation.
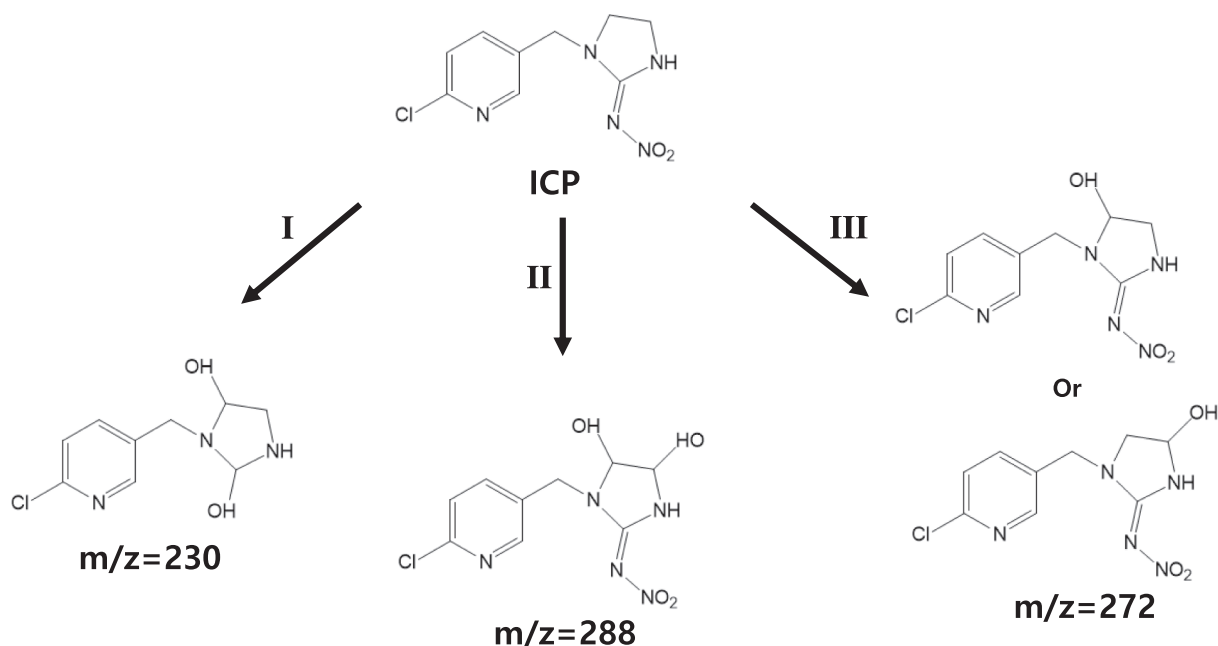
Fig. 11. The degradation pathways of ICP by SO_4-Ag_3PO_4 under visible light irradiation.

required for photoactivation and improve the charge transfer efficiency compared with the pristine Ag_3PO_4. Neonicotinoid insecticides were effectively degraded photocatalytically by SO_4-Ag_3PO_4 under visible light and their degradation rates varied depending on the insecticides in the order of TCP > NTP > ICP > CTD > ATP > TMX > DTF. The removal efficiency following 10 min irradiation cycles was maintained over 75% during the four reuse cycles, although performance was significantly hindered by background organics present in secondary effluent and lake water. Scavenger tests confirm that the photoinduced holes (h^+) are the most important oxidants in ICP degradation by SO_4-Ag_3PO_4, and the more efficient electron-h^+ pair separation efficiency explains the higher photocatalytic activity of SO_4-Ag_3PO_4 than Ag_3PO_4. Overall, this study demonstrates that the enhanced photocatalytic activity of SO_4-Ag_3PO_4 improved the removal efficiency of recalcitrant insecticides and that this material could be used to remove various water contaminants using solar irradiation, pending verification that adequate treatment time and intensity are provided to ensure not only regulatory compliance for residual concentrations, but also efficient detoxification.

Declaration of Competing Interest

The authors declare that they have no known competing financial interests or personal relationships that could have appeared to influence the work reported in this paper.

Acknowledgements

Appendix A. Supplementary data

Supplementary data to this article can be found online at https://doi.org/10.1016/j.cej.2020.126183.

References

[1] K. Yin, Y. Deng, C. Liu, Q. He, Y. Wei, S. Chen, T. Liu, S. Luo, Kinetics, pathways and toxicity evaluation of neonicotinoid insecticides degradation via UV/chlorine process, Chem. Eng. J. 346 (2018) 298–306.
[2] S.A. Todey, A.M. Fallon, W.A. Arnold, Neonicotinoid insecticide hydrolysis and photolysis: Rates and residual toxicity, Environ. Toxicol. Chem. 37 (2018) 2797–2809.
[3] R. Zabar, T. Komel, J. Fabjan, M.B. Kralj, P. Trebse, Photocatalytic degradation with immobilised TiO(2) of three selected neonicotinoid insecticides: imidacloprid, thiamethoxam and clothianidin, Chemosphere 89 (2012) 293–301.
[4] P. Jeschke, R. Nauen, M. Schindler, A. Elbert, Overview of the status and global strategy for neonicotinoids, J. Agric. Food Chem. 59 (2011) 2897–2908.
[5] D. Goulson, D. Kleijn, REVIEW: An overview of the environmental risks posed by neonicotinoid insecticides, J. Appl. Ecol. 50 (2013) 977–987.
[6] G. Rodriguez-Castillo, M. Molina-Rodriguez, J.C. Cambronero-Heinrichs, J.P. Quiros-Fournier, V. Lizano-Fallas, C. Jimenez-Rojas, M. Masis-Mora, V. Castro-Gutierrez, I. Mata-Araya, C.E. Rodriguez-Rodriguez, Simultaneous removal of neonicotinoid insecticides by a microbial degrading consortium: Detoxification at reactor scale, Chemosphere 235 (2019) 1097–1106.
[7] Y. Yao, C. Huang, Y. Yang, M. Li, B. Ren, Electrochemical removal of thiamethoxam using three-dimensional porous PbO2-CeO2 composite electrode: Electrode characterization, operational parameters optimization and degradation pathways, Chem. Eng. J. 350 (2018) 960–970.
[8] S. Raut-Jadhav, V.K. Saharan, D. Pinjari, S. Sonawane, D. Saini, A. Pandit, Synergetic effect of combination of AOP's (hydrodynamic cavitation and H(2)O(2)) on the degradation of neonicotinoid class of insecticide, J. Hazard. Mater. 261 (2013) 139–147.
[9] S. Chen, J. Deng, Y. Deng, N. Gao, Influencing factors and kinetic studies of imidacloprid degradation by ozonation, Environ. Technol. 40 (2019) 2127–2134.
[10] J.L. Acero, F.J. Real, F. Javier Benitez, E. Matamoros, Degradation of neonicotinoids by UV irradiation: Kinetics and effect of real water constituents, Sep. Purif. Technol. 211 (2019) 218–226.
[11] E. Shi, Z. Xu, W. Wang, Y. Xu, Y. Zhang, X. Yang, Q. Liu, T. Zeng, S. Song, Y. Jiang, L. Li, V.K. Sharma, Ag2S-doped core-shell nanostructures of Fe3O4@Ag3PO4 ultrathin film: Major role of hole in rapid degradation of pollutants under visible light irradiation, Chem. Eng. J. 366 (2019) 123–132.
[12] S.K. Loeb, P.J.J. Alvarez, J.A. Brame, E.L. Cates, W. Choi, J. Crittenden, D.D. Dionysiou, Q. Li, G. Li-Puma, X. Quan, D.L. Sedlak, T. David Waite, P. Westerhoff, J.H. Kim, The Technology Horizon for Photocatalytic Water Treatment: Sunrise or Sunset? Environ. Sci. Technol. 53 (2019) 2937–2947.
[13] L. Liu, Y. Qi, J. Lu, S. Lin, W. An, Y. Liang, W. Cui, A stable Ag 3 PO 4 @g-C 3 N 4 hybrid core@shell composite with enhanced visible light photocatalytic degradation, Appl. Catal. B-Environ. 183 (2016) 133–141.
[14] Z. Yi, J. Ye, N. Kikugawa, T. Kako, S. Ouyang, H. Stuart-Williams, H. Yang, J. Cao, W. Luo, Z. Li, Y. Liu, R.L. Withers, An orthophosphate semiconductor with photooxidation properties under visible-light irradiation, Nat. Mater. 9 (2010) 559–564.
[15] Y. Bi, S. Ouyang, N. Umezawa, J. Cao, J. Ye, Facet effect of single-crystalline Ag3PO4 sub-microcrystals on photocatalytic properties, J. Am. Chem. Soc. 133 (2011) 6490–6492.
[16] L. Song, J. Yang, S. Zhang, Enhanced photocatalytic activity of Ag3PO4

photocatalyst via glucose-based carbonsphere modification, Chem. Eng. J. 309 (2017) 222–229.

[17] W. Cao, Z. Gui, L. Chen, X. Zhu, Z. Qi, Facile synthesis of sulfate-doped Ag3PO4 with enhanced visible light photocatalystic activity, Appl. Catal. B-Environ. 200 (2017) 681–689.

[18] M. Sun, Q. Zeng, X. Zhao, Y. Shao, P. Ji, C. Wang, T. Yan, B. Du, Fabrication of novel g-C3N4 nanocrystals decorated Ag3PO4 hybrids: Enhanced charge separation and excellent visible-light driven photocatalytic activity, J. Hazard. Mater. 339 (2017) 9–21.

[19] Q. Xiang, D. Lang, T. Shen, F. Liu, Graphene-modified nanosized Ag3PO4 photocatalysts for enhanced visible-light photocatalytic activity and stability, Appl. Catal. B-Environ. 162 (2015) 196–203.

[20] Y. Li, P. Wang, C. Huang, W. Yao, Q. Wu, Q. Xu, Synthesis and photocatalytic activity of ultrafine Ag3PO4 nanoparticles on oxygen vacated TiO2, Appl. Catal. B-Environ. 205 (2017) 489–497.

[21] C.G. Lee, H. Javed, D. Zhang, J.H. Kim, P. Westerhoff, Q. Li, P.J.J. Alvarez, Porous electrospun fibers embedding TiO2 for adsorption and photocatalytic degradation of water pollutants, Environ. Sci. Technol. 52 (2018) 4285–4293.

[22] K. Huang, Y. Lv, W. Zhang, S. Sun, B. Yang, F. Chi, S. Ran, X. Liu, One-step synthesis of Ag3PO4/Ag photocatalyst with visible-light photocatalytic Activity, Mater. Res. 18 (2015) 939–945.

[23] J. Yan, C. Wang, H. Xu, Y. Xu, X. She, J. Chen, Y. Song, H. Li, Q. Zhang, AgI/ Ag3PO4 heterojunction composites with enhanced photocatalytic activity under visible light irradiation, Appl. Surf. Sci. 287 (2013) 178–186.

[24] Y. He, L. Zhang, B. Teng, M. Fan, New application of Z-scheme Ag3PO4/g-C3N4 composite in converting CO2 to fuel, Environ. Sci. Technol. 49 (2015) 649–656.

[25] M. Xie, T. Zhang, One-pot, facile fabrication of a Ag3PO4-based ternary Z-scheme photocatalyst with excellent visible-light photoactivity and anti-photocorrosion performance, Appl. Surf. Sci. 436 (2018) 90–101.

[26] S. Zhang, S. Zhang, L. Song, Super-high activity of Bi3+ doped Ag3PO4 and enhanced photocatalytic mechanism, Appl. Catal. B-Environ. 152–153 (2014) 129–139.

[27] G. Zhang, Y.C. Zhang, M. Nadagouda, C. Han, K. O'Shea, S.M. El-Sheikh, A.A. Ismail, D.D. Dionysiou, Visible light-sensitized S, N and C co-doped polymorphic TiO2 for photocatalytic destruction of microcystin-LR, Appl. Catal. B-Environ. 144 (2014) 614–621.

[28] W.J. Jo, J.W. Jang, K.J. Kong, H.J. Kang, J.Y. Kim, H. Jun, K.P. Parmar, J.S. Lee, Phosphate doping into monoclinic BiVO4 for enhanced photoelectrochemical water oxidation activity, Angew. Chem. 51 (2012) 3147–3151.

[29] E. Serrano, M. Munoz, Z.M. de Pedro, J.A. Casas, Fast oxidation of the neonicotinoid pesticides listed in the EU Decision 2018/840 from aqueous solutions, Sep. Purif. Technol. 235 (2020) 116168.

[30] N. Banić, B. Abramović, J. Krstić, D. Šojić, D. Lončarević, Z. Cherkezova-Zheleva, V. Guzsvány, Photodegradation of thiacloprid using Fe/TiO2 as a heterogeneous photo-Fenton catalyst, Appl. Catal. B-Environ. 107 (2011) 363–371.

[31] N.D. Banić, B.F. Abramović, D.V. Šojić, J.B. Krstić, N.L. Finčur, I.P. Bočković, Efficiency of neonicotinoids photocatalytic degradation by using annular slurry reactor, Chem. Eng. J. 286 (2016) 184–190.

[32] U. Cernigoj, U.L. Stangar, J. Jirkovsky, Effect of dissolved ozone or ferric ions on photodegradation of thiacloprid in presence of different TiO2 catalysts, J. Hazard. Mater. 177 (2010) 399–406.

[33] C. Feng, G. Xu, X. Liu, Photocatalytic degradation of imidacloprid by composite catalysts H3PW12O40/La-TiO2, J. Rare Earths 31 (2013) 44–48.

[34] F. Soltani-nezhad, A. Saljooqi, T. Shamspur, A. Mostafavi, Photocatalytic degradation of imidacloprid using GO/Fe3O4/TiO2-NiO under visible radiation: Optimization by response level method, Polyhedron 165 (2019) 188–196.

[35] R.A. Torres-Palma, J.I. Nieto, E. Combet, C. Petrier, C. Pulgarin, An innovative ultrasound, Fe(2+) and TiO(2) photoassisted process for bisphenol A mineralization, Water Res. 44 (2010) 2245–2252.

[36] M.F. Khan, L. Yu, G. Achari, J.H. Tay, Degradation of sulfolane in aqueous media by integrating activated sludge and advanced oxidation process, Chemosphere 222 (2019) 1–8.

[37] A. Carabin, P. Drogui, D. Robert, Photocatalytic Oxidation of Carbamazepine: Application of an Experimental Design Methodology, Water Air Soil Pollut. 227 (2016).

[38] S. Kurwadkar, A. Evans, D. DeWinne, P. White, F. Mitchell, Modeling photodegradation kinetics of three systemic neonicotinoids-dinotefuran, imidacloprid, and thiamethoxam-in aqueous and soil environment, Environ. Toxicol. Chem. 35 (2016) 1718–1726.

[39] R. Liang, F. Tang, J. Wang, Y. Yue, Photo-degradation dynamics of five neonicotinoids: Bamboo vinegar as a synergistic agent for improved functional duration, PloS one 14 (2019) e0223708.

[40] P. Dong, Y. Wang, B. Cao, S. Xin, L. Guo, J. Zhang, F. Li, Ag3PO4/reduced graphite oxide sheets nanocomposites with highly enhanced visible light photocatalytic activity and stability, Appl. Catal. B-Environ. 132–133 (2013) 45–53.

[41] W.S. Wang, H. Du, R.X. Wang, T. Wen, A.W. Xu, Heterostructured Ag3PO4/AgBr/ Ag plasmonic photocatalyst with enhanced photocatalytic activity and stability under visible light, Nanoscale 5 (2013) 3315–3321.

[42] F. Chen, Q. Yang, X. Li, G. Zeng, D. Wang, C. Niu, J. Zhao, H. An, T. Xie, Y. Deng, Hierarchical assembly of graphene-bridged Ag3PO4/Ag/BiVO4 (040) Z-scheme photocatalyst: An efficient, sustainable and heterogeneous catalyst with enhanced visible-light photoactivity towards tetracycline degradation under visible light irradiation, Appl. Catal. B-Environ. 200 (2017) 330–342.

[43] D. Zhang, C. Lee, H. Javed, P. Yu, J.H. Kim, P.J.J. Alvarez, Easily-recoverable, micron-sized TiO2 hierarchical spheres decorated with cyclodextrin for enhanced photocatalytic degradation of organic micropollutants, Environ. Sci. Technol. 12402–12411 (2018).

[44] W. Cao, Y. An, L. Chen, Z. Qi, Visible-light-driven Ag2MoO4/Ag3PO4 composites with enhanced photocatalytic activity, J. Alloy. Compd. 701 (2017) 350–357.

[45] H. Katsumata, M. Taniguchi, S. Kaneco, T. Suzuki, Photocatalytic degradation of bisphenol A by Ag3PO4 under visible light, Catal. Commun. 34 (2013) 30–34.

[46] X.-Q. Liu, W.-J. Chen, H. Jiang, Facile synthesis of Ag/Ag 3 PO 4 /AMB composite with improved photocatalytic performance, Chem. Eng. J. 308 (2017) 889–896.

[47] S. Thiyagarajan, S. Singh, D. Bahadur, Reusable sunlight activated photocatalyst Ag3PO4 and its significant antibacterial activity, Mater. Chem. Phys. 173 (2016) 385–394.

[48] M.L. Dell'Arciprete, L. Santos-Juanes, A. Arques, R.F. Vercher, A.M. Amat, J.P. Furlong, D.O. Mártire, M.C. Gonzalez, Reactivity of neonicotinoid pesticides with singlet oxygen, Catal. Today 151 (2010) 137–142.

[49] W. Han, D. Li, M. Zhang, H. Ximin, X. Duan, S. Liu, S. Wang, Photocatalytic activation of peroxymonosulfate by surface-tailored carbon quantum dots, J Hazard Mater 395 (2020) 122695.

[50] P. Tan, X. Chen, L. Wu, Y.Y. Shang, W. Liu, J. Pan, X. Xiong, Hierarchical flower-like SnSe2 supported Ag3PO4 nanoparticles: Towards visible light driven photocatalyst with enhanced performance, Appl. Catal. B-Environ. 202 (2017) 326–334.

[51] X. Jiang, D. Song, D. Wang, R. Zhang, Q. Fang, H. Sun, F. Kong, Eliminating imidacloprid and its toxicity by permanganate via highly selective partial oxidation, Ecotox. Environ. Safe. 191 (2020) 110234.

[52] G. Rózsa, M. Náfrádi, T. Alapi, K. Schrantz, L. Szabó, L. Wojnárovits, E. Takács, A. Tungler, Photocatalytic, photolytic and radiolytic elimination of imidacloprid from aqueous solution: Reaction mechanism, efficiency and economic considerations, Appl. Catal. B-Environ. 250 (2019) 429–439.